Optimization of the First Dirichlet Laplacian Eigenvalue with Respect to a Union of Balls

E. G. Birgin[1] · L. Fernandez[2] · G. Haeser[2] · A. Laurain[2]

Abstract

The problem of minimizing the first eigenvalue of the Dirichlet Laplacian with respect to a union of m balls with fixed identical radii and variable centers in the plane is investigated in the present work. The existence of a minimizer is shown and the shape sensitivity analysis of the eigenvalue with respect to the centers' positions is presented. With this tool, the derivative of the eigenvalue is computed and used in a numerical algorithm to determine candidates for minimizers. Candidates are also constructed by hand based on regular polygons. Numerical solutions contribute in at least three aspects. They corroborate the idea that some of the candidates based on regular polygons might be optimal. They also suggest alternative regular patterns that improve solutions associated with regular polygons. Lastly and most importantly, they delivered better quality solutions that do not follow any apparent pattern. Overall, for low values of m, candidates for minimizers of the eigenvalue are proposed and their geometrical properties as well as the appearance of regular patterns formed by the centers are discussed.

✉ E. G. Birgin
egbirgin@ime.usp.br

L. Fernandez
fernandez@ime.usp.br

G. Haeser
ghaeser@ime.usp.br

A. Laurain
laurain@ime.usp.br

[1] Department of Computer Science, Institute of Mathematics and Statistics, University of São Paulo, Rua do Matão, 1010, Cidade Universitária, São Paulo, SP 05508-090, Brazil

[2] Department of Applied Mathematics, Institute of Mathematics and Statistics, University of São Paulo, Rua do Matão, 1010, Cidade Universitária, São Paulo, SP 05508-090, Brazil

1 Introduction

Optimization of eigenvalues with respect to geometrical features is a topic of high interest in pure and applied mathematics but also in engineering and natural sciences, such as in structural mechanics for the control of vibration frequency [3], in mathematical biology [30, 35], acoustics [6, 20] or electromagnetism [2]. We refer to the book [27] of Henrot for a thorough overview of the topic.

The optimization of Laplacian eigenvalues is a popular topic in Mathematics as these problems are often simple and elegant to formulate, but are also challenging and require deep mathematical tools from a large spectrum of disciplines such as partial differential equations, spectral theory and differential geometry. The celebrated Rayleigh–Faber–Krahn inequality, conjectured by Lord Rayleigh in the nineteenth century and proved several decades later by Faber and Krahn, states that the ball minimizes the first Dirichlet eigenvalue under a volume constraint. Since then, many shape optimization problems of this nature have been considered, such as the minimization of the kth eigenvalue of the Dirichlet Laplacian [7, 16] for $k > 2$, or the minimization of eigenvalues with other types of partial differential equations (PDEs) and boundary conditions [17, 27]. Shape optimization of eigenvalues under geometric constraints has also attracted significant interest over the years in the literature: perimeter constraint [21], convexity constraint for the second Dirichlet eigenvalue [28], box constraint [27], diameter constraint [13], minimization in the class of polygons with at most n edges [12, 27] and optimal partition problems [14, 15].

Another type of geometric constraint that has not been much investigated in the shape optimization literature is to optimize with respect to a domain defined as a union of sets. In the engineering literature, the method of *Moving Morphable Component/Void* (MMC/MMV) [25, 42] has been developed recently to tackle such problem. Its goal is to achieve shape and topology optimization using a union of sets (the so-called *components/voids*) whose geometrical features can be controlled explicitly. The sensitivity analysis in this approach is usually formal and based on regularization, and a rigorous mathematical analysis, with or without using regularization, is lacking.

In the present paper we propose an initial foray into the rigorous mathematical analysis of this type of constraint, and consider numerical approximations employing domains with sharp interfaces, i.e., without regularization. We propose to investigate the minimization of the first Dirichlet eigenvalue when the domain is a union of m balls with fixed identical radii and variable centers in the plane. This naturally yields a well-posed minimization that raises interesting challenges. When considering domains defined as a union of sets, the union of balls is a natural contender with various applications in computational biology, molecular modeling, robotics [1, 23] and covering problems [8, 10]. In [8–10] shape optimization problems where the set to be optimized is a union of balls have already been considered. However, in these works the minimization problem does not depend on the solution of a PDE. When the cost functional

depends on the solution of a PDE, specific issues arise. A particularly important feature is the regularity of the solution and the appearance of singularities near the re-entrant corners that inevitably occur when working with a union of smooth sets, as described by the theory of corner singularities [19, 34, 38]. The low regularity of the solution of the PDE that ensues from these singularities complicates the shape sensitivity analysis and the numerical approximation of a minimizer. Shape optimization in the presence of singularities has been investigated for elliptic problems on nonsmooth domains, such as polygonal and Lipschitz domains, in [36, 37]. It also plays an important role in solid mechanics, for instance for the modeling of cracks, e.g., in [24, 33], where the classical Hadamard formula for the shape gradient is extended to nonsmooth domains, or for the topological optimization of structures subject to stress constraints [5].

In eigenvalue optimization with respect to the geometry, the first step is usually to determine geometric properties of the minimizer and, if possible, to find a plausible candidate for the minimizer. The second step is then to prove, or disprove, that this candidate is indeed a minimizer. For instance, for the minimization of the first Dirichlet eigenvalue under a volume constraint, it was first conjectured by Lord Rayleigh that the solution was a ball, and the conjecture was proved later on. For the minimization of the first Dirichlet eigenvalue of the Laplacian in the class of polygons with n edges and fixed volume, known as the Pólya conjecture, it is conjectured that the solution is the regular polygon with n edges, and an important step towards proving this conjecture has been obtained recently in [12]. However, the exact minimizer is sometimes difficult to guess or to describe explicitly. For instance, for the minimization of the second Dirichlet eigenvalue with a convexity constraint on the plane, it was first conjectured that the solution was the convex hull of two identical tangent balls, but this result was disproved later in [28].

For the problem investigated in the present paper, several familiar arguments from Dirichlet eigenvalue optimization may be considered to identify potential candidates. For instance, in light of the Rayleigh–Faber–Krahn inequality, it is reasonable to expect that the minimizer is simply connected and that the balls tend to agglomerate to approximate a larger ball. The balls' centers should form several layers, and a natural question is to ask how the structure of these layers depends on m and whether regular patterns appear. For low values of m, configurations following a regular polygonal pattern or aligned with a regular hexagonal lattice are natural candidates for minimizers. However, for specific values of m a plausible candidate may be difficult to guess, or several candidates may be competing.

Numerical investigations are then key to observe regular pattern formations in the minimizers and to establish conjectures. For this purpose we propose an algorithm based on shape optimization techniques [22, 29, 39] to approximate the minimizers. The union of balls can be seen as a nonsmooth set, a curvilinear polygon to be more precise, and a small perturbation of the centers' positions generates a geometric perturbation of this nonsmooth set. Under appropriate conditions on the balls' positions, this geometrical perturbation may be parameterized by a bi-Lipschitz mapping between the reference and the perturbed domains; here we can use the mapping that was constructed in [8, 10] for covering problems. This shape sensitivity analysis allows us eventually to compute the gradient of the eigenvalue with respect to the centers' positions, via the computation of the eigenvalue derivative with respect to the shape.

The eigenvalue gradient is then used in a numerical algorithm to approximate the minimizers. However, the computation of an accurate gradient is a challenging numerical problem, specially nearby regular patterns, where the computation of the gradient may be unstable. Thus, we use a standard steepest descent algorithm with Armijo's line search and we proceed to perform a block coordinate search heuristic, which can still make use of some of the gradient's components when the full gradient is not reliable, which was shown to improve the quality of the solution found. We conduct experiments by considering the problem with up to ten balls, where we start by guessing regular patterns which may provide good candidate solutions. These regular pattern solutions are then compared with the ones found by our algorithm starting from random initial points. In general, the algorithm finds solutions which are similar to the ones obtained with regular patterns, which suggests for some values of m that the regular pattern solutions are indeed minimizers; in some cases, the solution found by the algorithm suggests other regular patterns to be tested. However, surprisingly, for five and ten balls, our algorithm finds non-regular solutions which are better than the ones found under regular patterns, indicating that the problem of minimizing the first Dirichlet Laplacian with respect to a union of balls may have some unexpected solutions depending on the number of balls considered.

The rest of this work is organized as follows. In Sect. 2 the eigenvalue minimization problem is introduced, existence of solutions is proved, and the shape sensitivity analysis of the eigenvalue is performed. Section 3 describes the considered optimization algorithm. Numerical experiments are given in Sect. 4. Conclusions and lines for future research are given in the last section.

Notation: The notation $|\cdot|$ is used for the Euclidian norm in $\mathbb{R}^n$. For a given set $\omega \subset \mathbb{R}^2$, $\partial\omega$ denotes its boundary, $\overline{\omega}$ its closure, int ω its interior, ω^c its complement, and ν denotes the unitary-norm normal vector to $\partial\omega$, pointing outwards of ω. Let $B(x_i, r)$ denote an open ball with center x_i and radius r. We use the notation ν_i for the normal vector to $\partial B(x_i, r)$, pointing outwards of $B(x_i, r)$, and τ_i for the unitary-norm tangent vector to $\partial B(x_i, r)$, pointing counterclockwise. The divergence of a vector field $V : \mathbb{R}^2 \to \mathbb{R}^2$ is denoted by div V, and its Jacobian matrix by DV. For a function $v : \omega \to \mathbb{R}$, the normal derivative on $\partial\omega$ is denoted $\partial_\nu v := \nabla v \cdot \nu$. The identity matrix in $\mathbb{R}^{2\times2}$ is denoted by I.

2 Problem Setting and Sensitivity Analysis

Let $\Omega \subset \mathbb{R}^2$ be a bounded open set,

$$H^1(\Omega) := \{v \in L^2(\Omega) \mid \nabla v \in L^2(\Omega)\} \text{ and } H_0^1(\Omega) := \{v \in H^1(\Omega) \mid v = 0 \text{ on } \partial\Omega\}.$$

The first Dirichlet Laplacian eigenvalue is defined as

$$\lambda(\Omega) := \min_{u \in H_0^1(\Omega)\setminus\{0\}} \frac{\displaystyle\int_\Omega |\nabla u|^2}{\displaystyle\int_\Omega u^2}.$$

The first eigenvalue is simple if Ω is a regular connected open set and positive, see [27, Theorem 1.2.5]. The corresponding eigenfunction u satisfies

$$-\Delta u = \lambda(\Omega)u \text{ in } \Omega, \tag{1}$$

$$u = 0 \text{ on } \partial\Omega, \tag{2}$$

and we impose the normalization condition $\|u\|_{L^2(\Omega)} = 1$.

In this paper we consider the following eigenvalue minimization problem:

$$\text{Minimize } \lambda(\boldsymbol{x}) \text{ with respect to } \boldsymbol{x} := \{x_i\}_{i=1}^m \in \mathbb{R}^{2m}, \tag{3}$$

where $\lambda(\boldsymbol{x}) := \lambda(\Omega(\boldsymbol{x}))$ denotes the solution to (1,2) with $\Omega = \Omega(\boldsymbol{x}) := \cup_{i=1}^m B(x_i, r)$, with m and r fixed, $x_i \in \mathbb{R}^2$ for all $i \in \mathcal{M} := \{1, \ldots, m\}$. We briefly explain why the minimizers of problem (3) are not trivial and produce an interesting geometrical configuration of the centers $\{x_i\}_{i=1}^m$; a more detailed discussion is provided at the beginning of Sect. 3. First, when $\boldsymbol{x}^\star := \{x_i^\star\}_{i=1}^m$ is a solution of problem (3), $\Omega(\boldsymbol{x}^\star)$ must be connected due to a monotonicity property of Dirichlet eigenvalues, see Theorem 2. Second, $\Omega(\boldsymbol{x}^\star)$ achieves an equilibrium between two competing tendencies. On one hand, $\Omega(\boldsymbol{x}^\star)$ strives to maximize its area, as the first Dirichlet eigenvalue tends to decrease as the area of the domain increases. On the other hand, $\Omega(\boldsymbol{x}^\star)$ seeks to minimize the angles (measured from the interior of $\Omega(\boldsymbol{x}^\star)$) at circle intersections, and to prevent small gaps from appearing, as these create strong singularities that increase the eingenvalue. Furthermore, considering that the minimizer of λ with respect to a free-form shape under a volume constraint is a ball due to the Rayleigh–Faber–Krahn inequality, see [27, Theorem 3.2.1], one expects the balls $B(x_i^\star, r)$ to agglomerate and approximate a large ball as $m \to \infty$, and to minimize their overlapping while avoiding gaps in $\Omega(\boldsymbol{x}^\star)$, i.e., $\Omega(\boldsymbol{x}^\star)$ should be simply connected. Note that the minimizing of overlapping is also typical of solutions of covering problems [8, 10, 18].

2.1 Existence of Solutions

In this section we discuss the existence of solutions for problem (3). For this purpose we will use a result of Šverak [40]; see also [27, Theorem 2.3.19]. We first recall the definition of Hausdorff distance for compact and open sets, following [27, Sect. 2.3.3].

Definition 1 (*Hausdorff convergence*) Let K_1, K_2 be two non-empty compact sets in $\mathbb{R}^2$ and set

$$d(x, K_1) := \inf_{y \in K_1} |y - x|, \text{ for all } x \in \mathbb{R}^2,$$

$$\rho(K_1, K_2) := \sup_{x \in K_1} d(x, K_2).$$

The Hausdorff distance of K_1 and K_2 is defined by

$$d^H(K_1, K_2) := \max(\rho(K_1, K_2), \rho(K_2, K_1)).$$

If Ω_1, Ω_2 are two open subsets of a (large) compact set K, then their Hausdorff distance is defined by:

$$d_H(\Omega_1, \Omega_2) := d^H(K \setminus \Omega_1, K \setminus \Omega_2).$$

The Hausdorff convergence of Ω_n to $\Omega^\star$ is denoted $\Omega_n \overset{H}{\to} \Omega^\star$.

For any set $\mathcal{D} \subset \mathbb{R}^2$ open, let $\sharp \mathcal{D}^c$ denote the number of connected components of $\mathcal{D}^c$. The result of Šverak actually states the γ-convergence of Ω_n to Ω, but for the sake of simplicity we provide here a simpler statement dealing only with the first eigenvalue.

Theorem 1 (Šverak) *Let $K \subset \mathbb{R}^2$ be a fixed compact set and Ω_n a sequence of open subsets of K. Let p be a given integer and assume that the sets Ω_n satisfy $\sharp \Omega_n^c \leq p$ for all $n \in \mathbb{N}$. Then, if the sets Ω_n converge for the Hausdorff distance to a set Ω we have $\lambda(\Omega_n) \to \lambda(\Omega)$.*

We will also need the following monotonicity property for the inclusion for Dirichlet eigenvalues; see [27, Sect. 1.3.2].

Lemma 1 *Let Ω_1, Ω_2 be two bounded sets in $\mathbb{R}^2$ such that $\Omega_1 \subset \Omega_2$. Then $\lambda(\Omega_1) \leq \lambda(\Omega_2)$. Moreover, the inequality is strict as long as $\Omega_2 \setminus \Omega_1$ contains a set of positive capacity.*

Let $\{x_n\}_{n \in \mathbb{N}}$ be a minimizing sequence for problem (3), i.e., a sequence satisfying

$$\lambda(x_n) \to \inf_{x \in \mathbb{R}^{2m}} \lambda(x) \geq 0.$$

The key ingredient to prove existence of a solution to problem (3) is to apply Theorem 1, for which we need to prove the Hausdorff convergence of $\Omega(x_n)$ towards a set $\Omega(x^\star)$. However, $\Omega(x_n)$ does not always converge in the sense of Hausdorff to $\Omega(x^\star)$, but rather to a slightly larger set $\Omega^\dagger$ which is the union of $\Omega(x^\star)$ with a finite set of points. This allows us to show that $\lambda(\Omega^\dagger) = \lambda(\Omega(x^\star))$.

In what follows we will use

$$\mathcal{A}_i := \partial B(x_i, r) \cap \partial \Omega(x) \tag{4}$$

for $i \in \mathcal{M}$. Connected components of $\mathcal{A}_i$ are called *arcs* of $\partial \Omega(x)$; note that arcs are closed sets.

Theorem 2 *There exists $x^\star \in \mathbb{R}^{2m}$ solution of problem (3). In addition $\Omega(x^\star)$ is connected, it holds $|x_i^\star - x_j^\star| < 2mr$ for all $i, j \in \mathcal{M}$, and*

$$\min_{j \in \mathcal{M} \setminus \{i\}} |x_i^\star - x_j^\star| < 2r \text{ for all } i \in \mathcal{M}. \tag{5}$$

Proof Suppose that a minimizer $x^\star \in \mathbb{R}^{2m}$ exists and that $\Omega(x^\star)$ is not connected. Without loss of generality, we can assume that there are only two connected

components C_1 and C_2; the general case follows immediately. Then it is easy to see that $\lambda(C_1)$ and $\lambda(C_2)$ are both Dirichlet eigenvalues on $\Omega(x^\star)$ (but need not be the lowest Dirichlet eigenvalue). Without loss of generality we can also assume $\lambda(C_1) \leq \lambda(C_2)$. Since $\Omega(x^\star)$ has only two connected components, we have $\lambda(\Omega(x^\star)) = \min\{\lambda(C_1), \lambda(C_2)\} = \lambda(C_1)$; see [27, Remark 1.2.4]. Then, using Lemma 1, it is always possible to remove some ball $B(x_i^\star, r)$ from C_2 and add some ball $B(x_i, r)$ to C_1 so that $\lambda(C_1 \cup B(x_i, r)) < \lambda(C_1) = \lambda(\Omega(x^\star))$, which would contradict the fact that $x^\star$ is a minimizer. Thus $\Omega(x^\star)$ must be connected. The fact that $|x_i^\star - x_j^\star| < 2mr$ for all $i, j \in \mathcal{M}$ and (5) both follow immediately.

Let $\{x_n\}_{n \in \mathbb{N}}$ be a minimizing sequence for problem (3). Since $\lambda(x)$ is invariant by a uniform translation of the points x_i, i.e., $\lambda(x + \eta y) = \lambda(x)$ for all $\eta \in \mathbb{R}$, where $y := \{y_i\}_{i=1}^m \in \mathbb{R}^{2m}$ and $y_i = y \in \mathbb{R}^2$ for all $i \in \mathcal{M}$, we can assume that $x_{1,n} = (0, 0)$ is the origin, where $x_n = \{x_{i,n}\}_{i=1}^m$. We can also assume that $\Omega(x_n)$ is connected and that $|x_{i,n} - x_{j,n}| < 2mr$ for all $i, j \in \mathcal{M}$, for all $n \in \mathbb{N}$, otherwise if it is not the case for some n, we can substitute x_n with some y_n such that $\lambda(y_n) < \lambda(x_n)$, following the same reasoning used to show that $\Omega(x^\star)$ is connected. Thus $x_{i,n} \subset B((0, 0), 2mr)$ for all $i \in \mathcal{M}$ and all $n \in \mathbb{N}$. Hence we can extract a subsequence converging to some $x^\star$ such that $x_i^\star \subset \overline{B((0, 0), 2mr)}$ for all $i \in \mathcal{M}$. With a slight abuse of notation we also denote the subsequence by $\{x_n\}_{n \in \mathbb{N}}$.

Now we apply Theorem 1 to show that $\lambda(\Omega(x_n)) \to \lambda(\Omega(x^\star))$. To this end we need to show that there exists $p \in \mathbb{N}$ such that $\sharp\Omega(x_n)^c \leq p$ for all $n \in \mathbb{N}$. Let C be a connected component of $\Omega(x_n)^c$. Then ∂C is a finite union of arcs of $\partial\Omega(x_n)$. Also, two distinct connected components of $\Omega(x_n)^c$ can not have any arc in common. According to [31, Theorem 3.2] or [1, Theorem 2.2], $\partial\Omega(x)$ is the union of at most $6m - 12$ arcs. Thus, the number of connected components of $\Omega(x_n)^c$ is also bounded by $6m - 12$, independently of n.

Since $\Omega(x_n)$ is uniformly bounded, there exists $\Omega^\dagger$ and a subsequence of $\Omega(x_n)$, still denoted $\Omega(x_n)$ for simplicity, with $\Omega(x_n) \xrightarrow{H} \Omega^\dagger$; see [29, Corollary 2.2.26]. Since $B(x_{i,n}, r) \xrightarrow{H} B(x_i^\star, r)$ we have $\Omega(x^\star) = \cup_{i=1}^m B(x_i^\star, r) \subset \Omega^\dagger$; see [29, Sect. 2.2.3.2]. Then, introduce $\tilde{\Omega}_n = \cup_{i=1}^m B(x_i^\star, r + \epsilon_{i,n})$ with $\epsilon_{i,n} := |x_i^\star - x_{i,n}|$. We can take a subsequence, still denoted $\epsilon_{i,n}$, so that $\epsilon_{i,n} = |x_i^\star - x_{i,n}|$ is nonincreasing for all $i \in \mathcal{M}$. Thus $\tilde{\Omega}_n$ is nonincreasing with respect to the inclusion and using a property of [29, Sect. 2.2.3.2] we get $\tilde{\Omega}_n \xrightarrow{H} \text{int} \cup_{i=1}^m \overline{B(x_i^\star, r)}$. Also, we have $\Omega(x_n) \subset \tilde{\Omega}_n$, and since the Hausdorff convergence for open sets is stable for the inclusion, see [29, Sect. 2.2.3.2], we get $\Omega^\dagger \subset \text{int} \cup_{i=1}^m \overline{B(x_i^\star, r)}$. Hence, we have obtained

$$\Omega(x^\star) \subset \Omega^\dagger \subset \text{int} \cup_{i=1}^m \overline{B(x_i^\star, r)}.$$

Now observe that the difference between $\Omega(x^\star)$ and $\text{int} \cup_{i=1}^m \overline{B(x_i^\star, r)}$ is a finite set of points, thus

$$\lambda(\Omega(x^\star)) = \lambda(\Omega^\dagger) = \lambda(\text{int} \cup_{i=1}^m \overline{B(x_i^\star, r)}).$$

Finally we can apply Theorem 1, this shows that $\lambda(\Omega(x_n)) \to \lambda(\Omega^\dagger) = \lambda(\Omega(x^\star))$. Since x_n is a minimizing sequence, we get

$$\lambda(x^\star) = \min_{x \in \mathbb{R}^{2m}} \lambda(x),$$

and this shows that $x^\star \in \mathbb{R}^{2m}$ is a solution to problem (3).   □

2.2 Shape Sensitivity Analysis

In this section we compute the shape derivative of the first Dirichlet eigenvalue, under appropriate conditions on the balls' centers. The required condition, given in Assumption 1, is the same as in the shape sensitivity analysis for covering problem, see [8, 10]. It precludes balls from being tangent and from having the same centers. Also, any three circles can not intersect at the same point. In the covering problem, where no PDE was involved, these conditions were introduced for the sensitivity analysis, but it was shown in [8, 10] that the shape derivative often existed even when Assumption 1 was not satisfied. Here, the situation is more singular, and as x approaches a singular configuration, i.e., a configuration where Assumption 1 is not satisfied, one observes that the gradient of λ with respect to x also becomes singular. This phenomenon is due to the presence of corner singularities in the eigenfunction near the circles' intersections on $\partial\Omega(x)$; see [34, 38]. Note that in computational geometry, the circles $\partial B(x_i, r)$, $i \in \mathcal{M}$, satisfying Assumption 1 are said to be in *general position*; see [1].

Assumption 1 The centers $\{x_i\}_{i=1}^m$ satisfy $|x_i - x_j| \notin \{0, 2r\}$ for all $i, j \in \mathcal{M}, i \neq j$ and $\partial B(x_i, r) \cap \partial B(x_j, r) \cap \partial B(x_k, r) = \emptyset$ for all $i, j, k \in \mathcal{M}$ with i, j, k pairwise distinct.

Assumption 1 is used to obtain Theorem 3, a stability result on the structure of the boundary $\partial\Omega(x + t\delta x)$ with respect to t, where $\delta x := \{\delta x_i\}_{i=1}^m \in \mathbb{R}^{2m}$ is given. To be more precise, it allows us to show that $\partial\Omega(x + t\delta x)$ is the union of a fixed number of arcs for small t, i.e., that no new arcs appear and no arcs disappear. This allows us to build a bi-Lipschitz mapping $T_t : \overline{\Omega(x)} \to \mathbb{R}^2$ that is used to compute the shape derivative of $\Omega \mapsto \lambda(\Omega)$ using a change of variables. We omit the proof of Theorem 3 as it is essentially a particular case of [10, Theorem 2], except for the fact that the mapping T_t is only defined on $\partial\Omega(x)$ in [10, Theorem 2]. To show that $T_t : \overline{\Omega(x)} \to \mathbb{R}^2$ is a bi-Lipschitz mapping on the whole domain $\overline{\Omega(x)}$, one can proceed as in [8, Theorem 3.6].

Theorem 3 *Suppose that Assumption 1 holds. Then there exists $t_0 > 0$ such that for all $t \in [0, t_0]$ we have the following decomposition:*

$$\partial\Omega(x + t\delta x) = \bigcup_{k=1}^{\bar{k}} \mathcal{S}_k(t),   (6)$$

where $\mathcal{S}_k(t)$ are arcs parameterized by an angle aperture $[\theta_{k,v}(t), \theta_{k,w}(t)]$, $t \mapsto \theta_{k,v}(t)$, $t \mapsto \theta_{k,w}(t)$ are continuous functions on $[0, t_0]$, and $\bar{k}$ is independent of t.

Also, for all $t \in [0, t_0]$ there exists a bi-Lipschitz mapping $T_t : \overline{\Omega(x)} \to \mathbb{R}^2$ satisfying $T_t(\Omega(x)) = \Omega(x+t\delta x)$, $T_t(\partial\Omega(x)) = \partial\Omega(x+t\delta x)$ and $T_t(\mathcal{S}_k(0)) = \mathcal{S}_k(t)$ for all $k = 1, \ldots, \bar{k}$. Furthermore,

$$V \cdot v_i = \delta x_i \cdot v_i \ \text{on} \ \mathcal{S}_k(0) \cap \partial B(x_i, r), \ \text{for all} \ k = 1, \ldots, \bar{k}, \tag{7}$$

$$V(z) = \delta x_i - \frac{v_\ell(z) \cdot (\delta x_i - \delta x_\ell)}{\tau_i(z) \cdot v_\ell(z)} \tau_i(z) \quad \text{if} \ z \in \partial B(x_i, r) \cap \partial B(x_\ell, r), \ i \neq \ell, \tag{8}$$

where $V := \partial_t T_t|_{t=0}$.

Theorem 3 allows us to directly compute derivatives of shape functionals that do not depend on the solution of a PDE, as in [8, 10]. An additional step is required when the shape functional depends on the solution of a PDE however, as the regularity of the solution plays an important role for the existence of the derivative of the shape functional, and the analysis of the singularities appearing near the corners of $\partial\Omega(x)$ becomes a critical element. To this end, we need to discuss first some general regularity results for elliptic equations in curvilinear polygons.

Definition 2 (*Curvilinear polygons*) For $\ell \geq 2$, a bounded open subset $\mathcal{D} \subset \mathbb{R}^2$ is said to be a $\mathcal{C}^\ell$ *curvilinear polygon*, or more precisely a $\mathcal{C}^\ell$ *curvilinear κ-gon*, if it is Lipschitz, simply connected, and has a piecewise $\mathcal{C}^\ell$ boundary $\partial\mathcal{D} = \bigcup_{k\in\mathcal{K}} \overline{\Gamma_k}$, $\mathcal{K} := \{1, 2, \ldots, \kappa\}$, $\kappa \geq 2$, where Γ_k is a $\mathcal{C}^\ell$ open arc. Denoting $\Gamma_{\kappa+1} := \Gamma_1$, we define the vertex, or corner a_k as the common endpoint $a_k := \overline{\Gamma_k} \cap \overline{\Gamma_{k+1}}$, for $k \in \mathcal{K}$. The corner angle θ_k at a_k is the angle between the tangents to $\overline{\Gamma_k}$ and $\overline{\Gamma_{k+1}}$ at a_k, measured from the interior of $\mathcal{D}$. We assume that $0 < \theta_k < 2\pi$ and $\theta_k \neq \pi$ for all $k \in \mathcal{K}$. When Γ_k is a line segment for all $k \in \mathcal{K}$, then the curvilinear polygon $\mathcal{D}$ is called a polygon, or more precisely a κ-gon.

Let $K_{\theta,a}$ be a sector with opening angle $\theta \in (0, 2\pi]$ and vertex a, i.e.,

$$K_{\theta,a} = \{(r, \vartheta) : 0 < r < \infty, |\vartheta| < \theta/2\},$$

where $r := |x - a|$. Let $\mathbf{V}^s_{2,\gamma}(K_{\theta,a})$ be the weighted Sobolev space equipped with the norm

$$\|v\|_{\mathbf{V}^s_{2,\gamma}(K_{\theta,a})} := \left(\sum_{|\alpha| \leq s} \int_{K_{\theta,a}} r^{2(\gamma-s+|\alpha|)} \left| D^\alpha v(x) \right|^2 dx \right)^{1/2}.$$

Here $s \in \mathbb{N}$, $\alpha = (\alpha_1, \alpha_2)$ is a multi-index, $|\alpha| = \alpha_1 + \alpha_2$ and $D^\alpha v := \partial_1^{\alpha_1} \partial_2^{\alpha_2} v$. The idea behind the definition of $\mathbf{V}^s_{2,\gamma}(K_{\theta,a})$ is that the weight $r^{2(\gamma-s+|\alpha|)}$ allows for singularities in $D^\alpha v$: a larger value of γ allows for a stronger singularity in $D^\alpha v$; see [34, Sect. 6.1.1] and [38, Sect. 1.2.1].

The definition of $\mathbf{V}^s_{2,\gamma}(K_{\theta,a})$ is useful for a curvilinear polygon with a single vertex. One can extend this definition to the case of several vertices following [34, Sect. 6.2.1]. Let $\mathcal{D}$ be a $\mathcal{C}^\infty$ curvilinear polygon with vertices $a_k, k \in \mathcal{K}$. Assume that for all $k \in \mathcal{K}$,

there exists a neighbourhood $\mathcal{U}_k$ such that $\mathcal{D} \cap \mathcal{U}_k = K_{\theta_k,a_k} \cap \mathcal{U}_k$. Let ζ_k, $k \in \mathcal{K}$, be C^∞-functions in $\overline{\mathcal{D}}$ equal to one in a neighbourhood of a_k and to zero in $\overline{\mathcal{D}} \setminus \mathcal{U}_k$, and set $\zeta_0 = 1 - \sum_{k=1}^{\kappa} \zeta_k$. Let $H^s(\mathcal{D})$ denote the standard Sobolev space and define the weighted Sobolev space $\mathbf{V}_{2,\beta}^s(\mathcal{D})$, where $\beta = (\beta_1, \ldots, \beta_\kappa)$ is a vector of real numbers, as the set of all functions on $\mathcal{D}$ such that $\zeta_0 v \in H^s(\mathcal{D})$ and $\zeta_k v \in \mathbf{V}_{2,\beta_k}^s(K_{\theta_k,a_k})$, $k \in \mathcal{K}$. The space $\mathbf{V}_{2,\beta}^s(\mathcal{D})$ does not depend on the choice of the cut-off functions ζ_k and is equipped with the norm

$$\|v\|_{\mathbf{V}_{2,\beta}^s(\mathcal{D})} := \|\zeta_0 v\|_{H^s(\mathcal{D})} + \sum_{k=1}^{\kappa} \|\zeta_k v\|_{\mathbf{V}_{2,\beta_k}^s(K_{\theta_k,a_k})}.$$

Let $v \in H_0^1(\mathcal{D})$ be the solution to

$$-\Delta v = f \text{ in } \mathcal{D}, \tag{9}$$
$$v = 0 \text{ on } \partial\mathcal{D}. \tag{10}$$

The following lemma is a straightforward adaptation of [38, Theorem 1.3.2]. In [38], the boundary $\partial\mathcal{D}$ has only one vertex, but the result extends immediately to the case of several vertices. Roughly speaking, the singularity in the solution v of (9,10) is of order r^{π/θ_k} at the vertex a_k, so the singularity gets stronger as the angle θ_k (measured from the interior of $\mathcal{D}$) increases, and β_k needs to be chosen smaller as θ_k increases in order to obtain $\|\zeta_k v\|_{\mathbf{V}_{2,\beta_k}^s(K_{\theta_k,a_k})} < \infty$.

Lemma 2 *Suppose that $f \in \mathbf{V}_{2,\beta}^0(\mathcal{D})$ and $|\beta_k - 1| < \pi/\theta_k$ for all $k \in \mathcal{K}$. Then there exists a unique solution $v \in \mathbf{V}_{2,\beta}^s(\mathcal{D})$ of problem (9, 10) and the following estimate holds:*

$$\|v\|_{\mathbf{V}_{2,\beta}^2(\mathcal{D})} \le c \|f\|_{\mathbf{V}_{2,\beta}^0(\mathcal{D})}.$$

In our case the set $\Omega(x)$ is a curvilinear polygon if Assumption 1 holds, but $\Omega(x)$ does not coincide with a sector in the neighbourhood of the vertices a_k, $k \in \mathcal{K}$. However, in this case we can locally transform the boundary of $\partial\Omega(x)$ in a small neighbourhood of the vertices using a diffeomorphism, following the procedure described in [38, Sect. 1.3.7]. This yields the following result.

Lemma 3 *Suppose that Assumption 1 holds and that $|\beta_k - 1| < \pi/\theta_k$ for all $k \in \mathcal{K}$. Suppose that there exists a diffeomorphism $\psi : \mathcal{U}(\overline{\Omega(x)}) \mapsto \mathbb{R}^2$, where $\mathcal{U}(\overline{\Omega(x)})$ is a neighbourhood of $\overline{\Omega(x)}$, such that $\psi(a_k) = a_k$, $D\psi(a_k) = I$ and that there exists a neighbourhood $\mathcal{U}_k$ of a_k such that $\psi(\Omega(x) \cap \mathcal{U}_k) = K_{\theta_k,a_k} \cap \psi(\mathcal{U}_k)$ for all $k \in \mathcal{K}$. Then the following estimate holds for the first eigenfunction u solution to (1,2):*

$$\|u \circ \psi^{-1}\|_{\mathbf{V}_{2,\beta}^2(\psi(\Omega))} \le c \|u \circ \psi^{-1}\|_{\mathbf{V}_{2,\beta}^0(\psi(\Omega))}.$$

We can now state the main result of this section, whose proof relies on the regularity results in weighted Sobolev spaces obtained for the eigenfunction u.

Theorem 4 *Suppose that Assumption* 1 *holds, then*

$$\nabla\lambda(\boldsymbol{x}) = -\left(\int_{\mathcal{A}_1} |\nabla u|^2 v_1, \ldots, \int_{\mathcal{A}_m} |\nabla u|^2 v_m\right)^{\top}. \tag{11}$$

Proof Since Assumption 1 holds, the set $\Omega(\boldsymbol{x} + t\delta\boldsymbol{x})$ is a curvilinear polygon and is Lipschitz for all $t \in [0, t_0]$ and t_0 sufficiently small. We use the notation $\Omega = \Omega(\boldsymbol{x})$ for simplicity. Let (λ_t, u_t) be the first Dirichlet eigenpair in the domain $\Omega(\boldsymbol{x} + t\delta\boldsymbol{x})$ with the normalization condition

$$\int_{\Omega(\boldsymbol{x}+t\delta\boldsymbol{x})} u_t^2 = 1. \tag{12}$$

Using the change of variable $x \mapsto T_t(x)$, where T_t is given by Theorem 3, the eigenvalue evaluated on the perturbed domain is

$$\lambda_t = \int_{\Omega(\boldsymbol{x}+t\delta\boldsymbol{x})} |\nabla u_t|^2 = \int_{\Omega} A(t)\nabla u^t \cdot \nabla u^t$$

with $u^t := u_t \circ T_t$ and $A(t) := (\det T_t)(DT_t)^{-1}(DT_t)^{-\top}$.

Adapting the results from [22, Theorem 4.1, p. 482] and [32, Lemma 2.16], we can show that $t \mapsto A(t)$ belongs to $\mathcal{C}^1([0, t_0]; \mathcal{C}^0(\Omega, \mathbb{R}^{d\times d}))$ and

$$A'(0) := \frac{dA}{dt}(0) = -DV - DV^{\top} + (\text{div } V)I, \tag{13}$$

and $V := \partial_t T_t|_{t=0}$. When Ω is of class $\mathcal{C}^k$, $k \geq 1$, it is shown in [39, Proposition 2.82] that $t^{-1}(u^t - u)$ converges strongly to $\dot{u}$ in $H_0^1(\Omega)$, where $\dot{u}$ is the so-called *material derivative* of u^t. The proof of [39, Proposition 2.82] extends straightforwardly to the case where Ω is Lipschitz.

Thus we may compute the derivative

$$\lambda' := \left.\frac{d\lambda_t}{dt}\right|_{t=0} = \int_{\Omega} A'(0)\nabla u \cdot \nabla u + 2\nabla u \cdot \nabla\dot{u}. \tag{14}$$

The eigenfunction u also satisfies the variational equation

$$\int_{\Omega} \nabla u \cdot \nabla v = \lambda \int_{\Omega} uv \quad \text{for all } v \in H_0^1(\Omega).$$

In particular we can choose the test function $v = \dot{u} \in H_0^1(\Omega)$ which yields

$$\int_{\Omega} \nabla u \cdot \nabla\dot{u} = \lambda \int_{\Omega} u\dot{u}. \tag{15}$$

Also, differentiating the normalization condition (12) after the change of variable $x \mapsto T_t(x)$, we get

$$\int_\Omega 2u\dot{u} + u^2 \operatorname{div} V = 0. \tag{16}$$

Combining (14), (15) and (16) we obtain

$$\lambda' = \int_\Omega A'(0)\nabla u \cdot \nabla u - \lambda u^2 \operatorname{div} V = \int_\Omega S_1 : DV.$$

with

$$S_1 := (|\nabla u|^2 - \lambda u^2)I - 2\nabla u \otimes \nabla u. \tag{17}$$

Now we prove that $S_1 \in W^{1,1}(\Omega, \mathbb{R}^{2\times 2})$. Since $u \in H_0^1(\Omega)$ we clearly have $S_1 \in L^1(\Omega, \mathbb{R}^{2\times 2})$. First we prove $DS_1 \in L^1(\Omega, \mathbb{R}^{2\times 2\times 2})$ using Lemma 3. We claim that the diffeomorphism ψ of Lemma 3 can be built as follows. Let $\mathcal{U}(\overline{\Omega})$ be a neighbourhood of $\overline{\Omega}$. Since Assumption 1 holds, for sufficiently small $\epsilon > 0$ the set $\Omega \cap B(a_k, \epsilon)$ is the epigraph of a piecewise smooth function in an appropriate coordinate system of origin a_k, and the graph of this function converges towards the graph of a sector $K_{\theta_k, a_k} \cap B(a_k, \epsilon)$ as $\epsilon \to 0$, where a_k and θ_k are the vertices and interior angles of the curvilinear polygon Ω, respectively; see Definition 2. Thus, we can find a smooth ψ in $\mathcal{U}(\overline{\Omega}) \cap B(a_k, \epsilon)$ such that $\psi(a_k) = a_k$, $\psi(\Omega \cap B(a_k, \epsilon)) = K_{\theta_k, a_k} \cap \psi(B(a_k, \epsilon))$ and $D\psi(a_k) = I$ for all $k \in \mathcal{K}$. In $\mathcal{U}(\overline{\Omega}) \setminus \cup_{k=1}^\kappa B(a_k, 2\epsilon)$, ψ is chosen as the identity. Then ψ can be smoothly extended to the transition region $\mathcal{U}(\overline{\Omega}) \cap (\cup_{k=1}^\kappa B(a_k, 2\epsilon))$.

Next, we can apply Lemma 3 since $\psi(\Omega)$ coincides, in a neighbourhood of a_k, with a sector K_{θ_k, a_k}. With $v := u \circ \psi^{-1}$, this yields the estimate

$$\|v\|_{\mathbf{V}_{2,\beta}^2(\psi(\Omega))} \leq c\|v\|_{\mathbf{V}_{2,\beta}^0(\psi(\Omega))} \tag{18}$$

with $|\beta_k - 1| < \pi/\theta_k$, for all $k \in \mathcal{K}$. Then we have, using the change of variable $x \mapsto \psi^{-1}(x)$,

$$\int_\Omega |D^2 u \nabla u| = \int_{\psi(\Omega)} |D^2 v \nabla v|\xi, \tag{19}$$

where $\xi := \det(D(\psi^{-1})) : \psi(\Omega) \to \mathbb{R}$ and for all $\delta > 0$, we can choose ϵ sufficiently small so that $\|\xi - 1\|_{L^\infty(\mathcal{U}(\overline{\psi(\Omega)}))} \leq \delta$. Applying (18), (19), using $1 = \sum_{k=0}^\kappa \zeta_k$, we get, using $r_k := |x - a_k|$,

$$\int_\Omega |D^2 u \nabla u| = \int_{\psi(\Omega)} \zeta_0 |D^2 v \nabla v|\xi + \sum_{k=1}^\kappa \int_{\psi(\Omega)} r_k^{1/2} r_k^{-1/2} \zeta_k |D^2 v \nabla v|\xi$$

$$\leq c \left(\int_{\psi(\Omega)} \zeta_0 |D^2 v|^2\right)^{1/2} \left(\int_{\psi(\Omega)} \zeta_0 |\nabla v|^2\right)^{1/2}$$

$$+ c \sum_{k=1}^{\kappa} \left(\int_{\psi(\Omega)} r_k \zeta_k |D^2 v|^2 \right)^{1/2} \left(\int_{\psi(\Omega)} r_k^{-1} \zeta_k |\nabla v|^2 \right)^{1/2}$$

$$\leq c \|\zeta_0 v\|_{H^2(\psi(\Omega))} \|\zeta_0 v\|_{H^1(\psi(\Omega))} + c \sum_{k=1}^{\kappa} \|\zeta_k v\|_{\mathbf{V}^2_{2,\frac{1}{2}}(K_{\theta_k, a_k})} \|\zeta_k v\|_{\mathbf{V}^0_{2,\frac{1}{2}}(K_{\theta_k, a_k})}$$

$$\leq c \|\zeta_0 v\|^2_{H^2(\psi(\Omega))} + c \sum_{k=1}^{\kappa} \|\zeta_k v\|^2_{\mathbf{V}^2_{2,\frac{1}{2}}(K_{\theta_k, a_k})},$$

where c denotes a generic constant. Further, using $\beta = (\frac{1}{2}, \frac{1}{2}, \ldots, \frac{1}{2})$, we get

$$\left(\int_{\Omega} |D^2 u \nabla u| \right)^2 \leq c \|v\|^2_{\mathbf{V}^2_{2,\beta}(\psi(\Omega))} \underbrace{\leq}_{(18)} c \|v\|^2_{\mathbf{V}^0_{2,\beta}(\psi(\Omega))}$$

$$\leq c \|\zeta_0 v\|^2_{L^2(\psi(\Omega))} + c \sum_{k=1}^{\kappa} \int_{\psi(\Omega)} r_k \zeta_k |v|^2$$

$$\leq c \|v\|^2_{L^2(\psi(\Omega))} \leq c \|u\|^2_{L^2(\Omega)}.$$

Thus $\nabla |\nabla u|^2 = 2D^2 u \nabla u \in L^1(\Omega, \mathbb{R}^2)$. In view of (17), we can treat the other terms of S_1 in a similar way and we conclude that $DS_1 \in L^1(\Omega, \mathbb{R}^{2 \times 2 \times 2})$ and $S_1 \in W^{1,1}(\Omega, \mathbb{R}^{2 \times 2})$.

Finally, using $S_1 \in W^{1,1}(\Omega, \mathbb{R}^{2 \times 2})$ and the fact that Ω is Lipschitz, we can apply [37, Proposition 1] which yields, using $u = 0$ on $\partial \Omega$,

$$\lambda' = \int_{\partial \Omega} (S_1 \nu) \cdot V = - \int_{\partial \Omega} |\partial_\nu u|^2 V \cdot \nu$$

Now, using (7) we get

$$\nabla \lambda(\boldsymbol{x}) \cdot \delta \boldsymbol{x} = \lambda' = - \sum_{i=1}^{m} \int_{\mathcal{A}_i} |\partial_\nu u|^2 V \cdot \nu_i = \sum_{i=1}^{m} \delta x_i \cdot \int_{\mathcal{A}_i} -|\partial_\nu u|^2 \nu_i$$

which yields (11). $\qquad\square$

Remark 1 Formula (11) for the gradient of λ has a similar structure as formula [8, (2.3)]. The main difference is the term $|\nabla u|^2$ in the integrals in (11). In [8, (2.3)], a derivative with respect to the radius r also appears, but in problem (3) the radius is fixed.

3 Optimization Processes

In this section we describe the practical implementation of the computation of the objective function of problem (3) and its derivatives. We also describe the optimization algorithms used in the attempt to solve problem (3).

3.1 Evaluation of the Objective Function and Its Gradient

Our numerical experiments were performed using the open-source software FreeFEM [26]. The finite element method was used to compute the eigenfunction with standard piecewise linear Lagrange elements for the discretization. The convergence analysis of finite element approximations to shape gradients for eigenvalue problems on polygons was performed in [43]. In order to evaluate the gradient $\nabla\lambda(x)$ given by (11), one must obtain the first eigenvector solution to (1,2) for a given $\Omega(x)$. Thus, for the numerical implementation and solution of problem (1,2), we consider the following main three steps: (i) determine the decomposition (6) into arcs of the boundary $\partial\Omega(x)$; (ii) generate a finite element mesh for $\Omega(x)$; (iii) compute $\lambda(x)$ and the corresponding approximate eigenfunction by solving the eigenvalue problem using a shifted-inverse power method and evaluate $\nabla\lambda(x)$.

To generate a finite element mesh for $\Omega(x)$, the mesh generation process in FreeFEM expects the boundary $\partial\Omega(x)$ as input, given as the parameterization of a closed curve or a union of connected closed components such as lines and arcs, for instance. The boundary of each connected component of $\Omega(x)$ may be itself composed of several connected components, that can be classified as either outer or inner boundary. This information must be provided for the mesh generation. In our case, $\partial\Omega(x)$ is a union of arcs $\mathcal{S}_k, k = 1, \ldots, \bar{k}$, see the decomposition (6). The mapping of these arcs is performed using the following numerical procedure, supposing Assumption 1 holds. For all $i, j \in \mathcal{M}$, we fix the ball $B(x_i, r)$ and verify if the condition $B(x_i, r) \cap B(x_j, r) \neq \emptyset$ holds for $j > i$. If the condition is satisfied, the intersection points of the two balls are computed, and a list of vertices of $\partial\Omega(x)$ is created by determining if an intersection point is on $\partial\Omega(x)$ or in $\Omega(x)$. Then we determine the connected components of $\partial\Omega(x)$ in the following way. For each circle $\partial B(x_i, r)$, the polar coordinates with pole x_i of the vertices belonging to $\partial B(x_i, r)$ are computed. This allows us to order the vertices on $\partial B(x_i, r)$. A first vertex is chosen randomly on some circle $\partial B(x_i, r)$. The next vertex on $\partial B(x_i, r)$ can then be found, moving along the circle using a counterclockwise orientation. This vertex belongs to some $\partial B(x_j, r)$ for some $j \neq i$, and we proceed to find the next vertex on $\partial B(x_j, r)$. This process is then repeated until the initial vertex is reached. This selects a set of vertices and determines the first connected component of $\partial\Omega(x)$. Next we repeat the process starting from a vertex that has not been selected yet, until no vertex is left. This eventually provides all connected components of $\partial\Omega(x)$. Each connected component of $\partial\Omega(x)$ is associated with a set of vertices which determines a polygon. Any two of these polygons either have an empty intersection or one is included in the other. Indeed, since each edge of these polygons is a segment connecting two consecutive intersection points on a circle, it can be seen that the edges of one polygon do not intersect the edges of the other. The empty intersection, or inclusion, of one polygon with the other polygons can be determined numerically using a ray casting algorithm. This allows us to determine, for each connected component of $\partial\Omega(x)$, whether it is an outer or an inner boundary of a connected component of $\Omega(x)$.

Next, the mesh generation is performed by using the command `buildmesh`. In addition to the data described above, the command `buildmesh` expects a num-

ber of subdivisions of each arc $\mathcal{S}_k$ of $\partial\Omega(\boldsymbol{x})$, $k = 1, \ldots, \bar{k}$, see (6). By defining a multiplicative factor $\zeta > 0$, and denoting by ϑ_k the angle aperture of the arc $\mathcal{S}_k$ (measured in degrees), the number of subdivisions for the discretization of $\mathcal{S}_k$ is $\mathrm{p}_k = \max(2, \lceil \zeta \vartheta_k \rceil)$. In this setting, the finite element mesh gets finer as ζ increases, and coarser as ζ gets closer to zero. For all numerical experiments in Sect. 4, we have considered $\zeta = 0.5$ which implies $\mathrm{p}_k = 2$ whenever $\vartheta_k < 2°$, and $\mathrm{p}_k = \lceil \zeta \vartheta_k \rceil$ otherwise. This choice of ζ guarantees a sufficiently fine mesh for the numerical approximations of solutions of partial differential equations and calculations of derivatives and integrals in this work, with the maximum edge size of the triangulation of $\Omega(\boldsymbol{x})$ given by $h_{\max} \approx 0.07$. Moreover, although optional parameters can be declared when calling the `buildmesh` function, the values of p_k, for $k = 1, \ldots, \bar{k}$, are the only values used for mesh generation in each of our numerical experiments.

The weak formulation of the PDE is then discretized using piecewise linear Lagrange elements and the eigenvalues and eigenvectors are obtained by calling the function `EigenValue`, which uses the shift-invert mode of the ARPACK++ library by default. In our numerical experiments, we have set the shift parameter of the method as zero for computing the first eigenvalue, while all other parameters are declared with their default values. The boundary integrals in the expression (11) of $\nabla\lambda(\boldsymbol{x})$ are then evaluated using the function `int1d`. As input parameters, function `int1d` requires the mesh of the triangulation of $\Omega(\boldsymbol{x})$, and the label corresponding to the arc (or the union of arcs) where the integration is to be performed. By default, on edges, FreeFEM uses the Gauss–Legendre quadrature formula with three nodes, which is exact for polynomials of degree at most five.

3.2 Steepest Descent and Block Coordinate Search

In this section we describe the two classical techniques of unconstrained minimization of differentiable functions which were used to minimize the function $\lambda(\boldsymbol{x})$ by exploiting the information available at its gradient $\nabla\lambda(\boldsymbol{x})$ as described in Sect. 3.1. Algorithm 1 describes the Gradient method or Steepest Descent method with the Armijo line search condition. Note that we use $\|\cdot\|_2$ and $\|\cdot\|_\infty$ for the Euclidean and infinity norms, respectively. Global convergence results can be shown for this method assuming only continuity of the gradient; see [11, Chap. 8]. The other technique described is the Block Coordinate Search method. To minimize a function of many variables, it is natural to keep some variables fixed and move others with the intention of decreasing the value of the objective function. This classical method works this idea in a systematic way, and it is having a renewed interest nowadays due to the fact that it can be applied to huge optimization problems such as those appearing in the areas of machine learning or statistical learning; see [4, 41]. However, this is not the reason why this method has been considered in this work, but rather because it proved to be useful to improve solutions found by the Gradient method. In particular, near a solution, the Gradient method frequently stopped possibly due to a lack of accuracy in the computation of the gradient, but it turns out that some of its components are still accurately computed and some further improvements may be achieved along these components.

Algorithm 1: STEEPEST DESCENT.

Input: Initial guess $x^0 \in \mathbb{R}^{2m}$, algorithmic constants $\gamma \in (0, 1)$, $0 < \sigma_1 \le \sigma_2 < 1$, and stopping
      criterion tolerance $\epsilon_g > 0$.
Output: $x^* \in \mathbb{R}^{2m}$.
1 $k \leftarrow 0$
2 **while** $\|\nabla\lambda(x^k)\|_\infty \not\le \epsilon_g$ **do**
3      $t \leftarrow 1$
4   **while** $\lambda(x^k - t\,\nabla\lambda(x^k)) \not\le \lambda(x^k) - t\gamma\|\nabla\lambda(x^k)\|_2^2$ **do**
5   define $t_{\text{new}} \in [\sigma_1\,t, \sigma_2\,t]$ and set $t \leftarrow t_{\text{new}}$.
6      $x^{k+1} := x^k - t\,\nabla\lambda(x^k)$
7      $k \leftarrow k + 1$
8 $x^* := x^k$
9 **Return** x^*

Algorithm 1 describes the considered Gradient method. In the algorithm, the calculation of t_{new} (line 5) uses safeguarded one-dimensional quadratic interpolation, i.e., we define

$$t_{\text{new}} \leftarrow \frac{t^2\|\nabla\lambda(x^k)\|_2^2}{\lambda(x^k - t\,\nabla\lambda(x^k)) - \lambda(x^k) + t\|\nabla\lambda(x^k)\|_2^2}$$

and if $t_{\text{new}} \notin [\sigma_1 t, \sigma_2 t]$, then we redefine $t_{\text{new}} \leftarrow t/2$, where $\sigma_1 = 0.1$ and $\sigma_2 = 0.9$. In practice, convergence to "singular" points at which the gradient is not well defined prevents the stopping criterion of Algorithm 1 from being satisfied. Therefore, additional stopping criteria are necessary. The simplest of all is to set a maximum of iterations $k_{\max} \ge 0$ and stop if $k \ge k_{\max}$. However, defining a practical value for $k_{\max}$ is difficult. In practice, when, at iteration k, $\nabla\lambda(x^k)$ does not correspond to a true gradient, what is observed is that Armijo's inner loop (lines 4 and 5) is satisfied only for very small, almost zero, values of t. When this happens, the consecutive iterates x^k and x^{k+1} are very close. Thus, the reasonable "lack of progress" stopping criterion becomes $\delta_k := \|x^{k+1} - x^k\|_\infty/\|x^k\|_\infty = t\,\|\nabla\lambda(x^k)\|_\infty/\|x^k\|_\infty \le \epsilon_x$ for some given tolerance $\epsilon_x > 0$ or, to be more conservative, if this occurs over several (say 5) consecutive iterations.

The solutions to problem (3) often display, or are close to, singular geometrical configurations, in the sense that Assumption 1 is not satisfied. In practice this means that the stopping condition $\|\nabla\lambda(x^k)\|_\infty \le \epsilon_g$ of Algorithm 1 is almost never satisfied and the algorithm stops due to the lack of progress stopping criterion $\delta_k \le \epsilon_x$. When that happens, the partial derivatives of λ with respect to some of the x_i's may not exist or may be different from (11). In such configurations, the partial derivatives of λ with respect to the x_i's that do not correspond to singularities are still correct, and this naturally calls for the application of a block coordinate search method. In Algorithm 2, we describe the method we employ after Algorithm 1 terminates. The key point of the algorithm is, at iteration k, by modifying only a subset $I_k \subseteq \mathcal{M}$ of the variables (balls' centers), to find an x^{k+1} that improves the value of the objective function (line 5). That is, what is sought at each iteration is $\lambda(x^{k+1}) < \lambda(x^k)$. In our implementation, we

search for x^{k+1} minimizing $\lambda(x)$ subject to $x_i = x_i^k$ for all $i \notin I_k$. More specifically, we try to just take a step in the direction of minus gradient (restricted to the coordinates being considered) that reduces the value of λ. If we denote

$$[\nabla_{I_k}\lambda(x)]_i = \begin{cases} [\nabla\lambda(x)]_i, & \text{if } i \in I_k, \\ 0, & \text{otherwise,} \end{cases}$$

then the calculation of x^{k+1} consists of a backtracking that starts with $t = 1$ and while $\lambda(x^k - t\,\nabla_{I_k}\lambda(x^k)) \geq \lambda(x^k)$, it computes a new step $t_{new} \in [\sigma_1 t, \sigma_2 t]$ and redefines $t = t_{new}$. In practice, a maximum of 5 reductions of t is allowed. In general, this strategy is well succeeded in finding x^{k+1} of the form $x^k - t\,\nabla_{I_k}\lambda(x^k)$ that satisfies $\lambda(x^{k+1}) < \lambda(x^k)$ in situations where the calculated partial derivatives coincide with true derivatives, and it fails in the other cases. If, at the end of a "cycle" (lines 3 to 7), no ball moved or the largest movement was considered small, the method stops. Of course, all this is just one possibility developed ad hoc within the many possibilities that the block coordinate search method encompasses. This algorithm was used as a heuristic method to try to improve the approximate solution calculated with the Steepest Descent method.

Algorithm 2: BLOCK COORDINATE SEARCH.

Input: Initial guess $x^0 \in \mathbb{R}^{2m}$ and stopping criterion tolerance $\epsilon_x > 0$.
Output: $x^* \in \mathbb{R}^{2m}$.
1 $k \leftarrow 0$
2 **do**
3 $\quad$ $\delta \leftarrow 0$
4 $\quad$ **for** $\ell = 1, \ldots, m$ **do**
5 $\quad\quad$ Find x^{k+1} such that $x_i^{k+1} = x_i^k$ for all $i \notin I_k \equiv \{\ell\}$ and $\lambda(x^{k+1}) \leq \lambda(x^k)$.
6 $\quad\quad$ Set $\delta \leftarrow \max(\delta, \|x^{k+1} - x^k\|_\infty / \|x^k\|_\infty)$.
7 $\quad\quad$ $k \leftarrow k + 1$
8 **while** $\delta > \epsilon_x$
9 $x^* := x^k$
10 **Return** x^*

---

4 Numerical Experiments

In this section we describe numerical experiments performed for the purpose of finding good quality solutions to problem (3) with m varying from 2 to 10. We begin the section with the description of ad hoc techniques for constructing solutions of problem (3) following regular polygonal patterns. The nonlinear approach is then described. We end the section with the construction of symmetric solutions inspired by the solutions obtained with the optimization process and a summary of the results.

We implemented the computation of the objective function and its gradient described in Sect. 3.1 and Algorithms 1 and 2 of Sect. 3.2 in FreeFEM. All tests were conducted on a computer with four 2.3 GHz AMD Opteron(tm) 6376 processors and

256GB 1866 MHz DDR3 RAM memory, running Debian 11. Code was compiled by the FreeFEM compiler (version 4.1) with the -nw no graphic option enabled.

4.1 Construction of Approximate Solutions Following Regular Patterns

In many eigenvalue optimization problems, the global optimizer can be guessed or a plausible candidate emerges from numerical experiments. For instance, in the case of the minimization of the second Dirichlet Laplacian eigenvalue with a convexity constraint, the so-called *stadium*, convex hull of two identical tangent disks, was at first considered as a candidate for minimizing the second eigenvalue, but this conjecture was disproved later on in [28]. For the minimization of the first eigenvalue in the class of n-gons, it has been proved for $n = 3, 4$ that the regular n-gon is the minimizer, and it is conjectured that the regular n-gon is also the minimizer for $n \geq 5$; see [27]. An important step towards proving this conjecture has been made recently in [12].

For problem (3) the optimizers may be difficult to foresee, but an educated guess can be made about them by pondering several arguments. First, as explained at the beginning of Sect. 2, one expects $\Omega(x^\star)$ to be simply connected and to converge towards a ball as $m \to \infty$, in some appropriate sense. For small values of m, the deviation from a ball could be relatively large. Second, $\Omega(x^\star)$ should display an equilibrium between maximizing its area, keeping $\Omega(x^\star)$ simply connected, and minimizing the angles (measured from the interior of $\Omega(x^\star)$) at the circles' intersections on $\partial\Omega(x^\star)$. Furthermore, since the thinnest covering of the plane is achieved by arranging the discs' centers in a regular hexagonal lattice; see [18, Chap. 2, p. 32], one expects that such lattice should play an important role for problem (3), as it allows to minimize the balls' overlapping without creating gaps in $\Omega(x^\star)$. For $m = 10$, we were able to construct a reasonable solution by placing the balls' centers on a regular hexagonal lattice, but our algorithm was able to find a better solution. However, we conjecture that the regular hexagonal lattice should play a significant role for larger values of m.

In view of the above discussion, it is natural for low values of m to consider arrangements of the centers $\{x_i\}_{i=1}^m$ following a regular polygonal pattern. As m increases, more balls need to be placed at the center and surrounded by an outer layer of balls. For m from 2 to 5 we considered configurations with the centers of the balls at the vertices of a regular polygon with m vertices and side L. For m between 6 and 10, we contemplated configurations with $m - 1$ balls centered at the vertices of a regular polygon of side L with $m - 1$ vertices and one ball centered at the polygon's center. Numerical experiments show that the case $m = 10$ is the limit case where it is more interesting to place two balls at the center. In such configurations, the value of L would be a variable to be determined. Since these are simple one-dimensional optimization problems, although more sophisticated approaches could be used, we opted for a brute-force search in an interval $[L_{\min}, L_{\max}]$. In other words, using the chain rule and expression (11) of $\nabla\lambda(x)$, the derivatives with respect to L could have been easily calculated, however, knowing that the solutions could be singular, we envisioned that brute force would be more appropriate.

In this experiment, as in the whole work, we considered balls of radius $r = 1$. We chose $L_{\min} = 1$ and $L_{\max} = 2$ and we tested all values of $L \in [L_{\min}, L_{\max}]$ of the
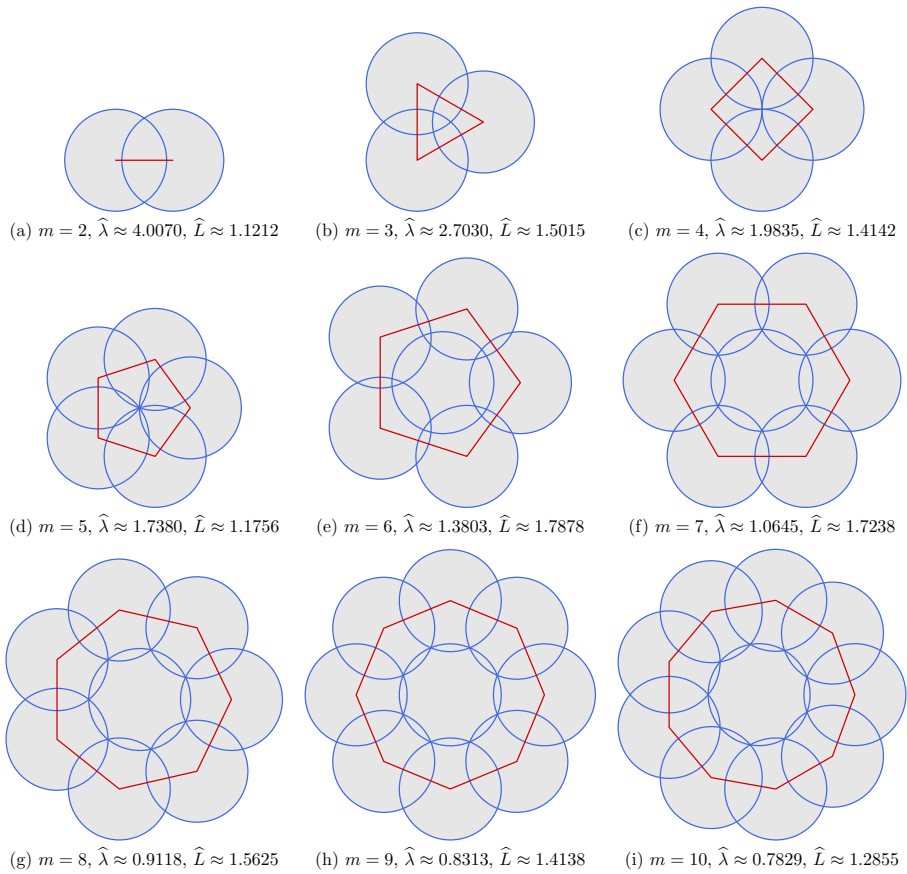
(a) $m = 2$, $\widehat{\lambda} \approx 4.0070$, $\widehat{L} \approx 1.1212$ (b) $m = 3$, $\widehat{\lambda} \approx 2.7030$, $\widehat{L} \approx 1.5015$ (c) $m = 4$, $\widehat{\lambda} \approx 1.9835$, $\widehat{L} \approx 1.4142$

(d) $m = 5$, $\widehat{\lambda} \approx 1.7380$, $\widehat{L} \approx 1.1756$ (e) $m = 6$, $\widehat{\lambda} \approx 1.3803$, $\widehat{L} \approx 1.7878$ (f) $m = 7$, $\widehat{\lambda} \approx 1.0645$, $\widehat{L} \approx 1.7238$

(g) $m = 8$, $\widehat{\lambda} \approx 0.9118$, $\widehat{L} \approx 1.5625$ (h) $m = 9$, $\widehat{\lambda} \approx 0.8313$, $\widehat{L} \approx 1.4138$ (i) $m = 10$, $\widehat{\lambda} \approx 0.7829$, $\widehat{L} \approx 1.2855$

Fig. 1 Best solutions found for $m \in \{2, 3, \ldots, 10\}$ following a regular polygonal pattern. The case $m = 2$ corresponds to the centers at the ends of a segment of size $\widehat{L}$. For the cases $m \in \{3, 4, 5\}$, the centers of the balls correspond to the vertices of a regular polygon with m vertices and side length $\widehat{L}$. For the cases $m \in \{6, \ldots, 10\}$, we considered regular polygons with $m - 1$ vertices and one ball is placed in the center of the polygon

form $L = L_{\min} + k\,h\,(L_{\max} - L_{\min})$ for $k = 0, 1, \ldots, N - 1$ and $h = 1/(N - 1)$. We considered $N = 10,000$. We denote by $\widehat{L}$ the best L found in this way, with a value $\widehat{\lambda}$ for the corresponding value of $\lambda(x)$ as depicted in Fig. 1.

4.2 Nonlinear Approach

Algorithm 1, with exact evaluation of the objective function and its derivatives, enjoys global convergence to stationary points of problem (3), i.e., independently of the initial guess, every limit point of the sequence generated by the algorithm nullifies the objective function's gradient. However, the inaccurate evaluation of the objective

function and the gradient does not allow small values of the gradient to be observed in practice. Therefore, for both Algorithms 1 and 2, the relevant tolerance is ϵ_x. For both algorithms we used $\epsilon_x = 10^{-4}$. Moreover, we are indeed interested in global minimizers of problem (3) and not in stationary points. That is why Algorithm 1 was embedded in a simple restarting technique in which the algorithm is run n_{trials} times starting from different initial points. In the experiments we considered $n_{\text{trials}} = 5,000$ for $m \leq 8$ and $n_{\text{trials}} = 50,000$ for $m = 9$ and $m = 10$. Preliminary results suggested the increase of n_{trials} for large m in order for the algorithm to achieve a reasonable solution. Only the best final point obtained by Algorithm 1 is improved using Algorithm 2.

The calculation of the random initial points used in Algorithm 1 requires an explanation. If in a configuration a ball does not overlap with any other ball, then the partial derivatives relative to its center are zero. Therefore, the position of such a ball is unlikely to change throughout the optimization process and the optimization algorithm will most likely converge to a suboptimal configuration, since Theorem 2 states that the optimal solution $\Omega(x^\star)$ must be connected. It is therefore recommended that the starting point x^0 generate a connected set $\Omega(x^0)$. The construction of the initial configuration considers a square of side L (we arbitrarily used $L = 1, 2, 3, 4, 4, 4, 4, 5, 5$ for $m = 2, 3, \ldots, 10$, respectively) within which the centers of the m balls are drawn with uniform distribution. After drawing the m centers, we check whether the configuration is connected. If it is not, the configuration is discarded and a new configuration is drawn. The connectivity check can be easily implemented with $O(m^2)$ time complexity. We start by marking the first ball as connected. Next, we calculate the distance from the first ball to the other balls and mark as connected those whose distance is less than twice the radius of the balls. Whenever this process marks new balls as connected, we repeat the process for the new balls. The configuration is connected if, when it stops, all balls were marked as connected.

Figure 2 and Table 1 show the solutions found. In the table, $\widehat{\lambda}$ corresponds to the solution found under regular polygonal patterns for comparison (as in Fig. 1), $\lambda_1^\star$ corresponds to the best λ found for each $m \in \{2, 3, 4, \ldots, 10\}$ after the execution of Algorithm 1, while $\lambda_2^\star$ corresponds to the improved value of λ obtained after the application of Algorithm 2, $\|\nabla\lambda_1^\star\|_2$ and $\|\nabla\lambda_2^\star\|_2$ correspond to the respective gradients' Euclidean norms, "#trial" indicates which initial guess (among the $n_{\text{trials}} = 5000$ or $50,000$) was the one that led to the best solution. Specifically for attempt #trial, "it" corresponds to the number of iterations of Algorithm 1, "fcnt" corresponds to the total number of evaluations of the objective function (on average, between 1 and 2 per iteration) and "CPU time" corresponds to the CPU time in seconds. "Average CPU time" corresponds to the average CPU time, in seconds, in relation to the n_{trials} attempts of Algorithm 1. The last three columns correspond to the number of "cycles", functional evaluations, and CPU time in seconds spent by Algorithm 2. By cycle, we mean a set of m iterations in which all x_i with $i \in \mathcal{M}$ are considered (see Algorithm 2). In fact, the number of iterations of Algorithm 2 corresponds to the number of cycles times $m - 1$ instead of times m, because in the optimization problem we consider x_1, the center of ball 1, fixed at the origin of the Cartesian plane as well as the first coordinate of x_2 null. That is, the optimization problems always have $2m - 3$ unknowns instead of $2m$. Overall, the total time of the experiment, which corresponds to adding the average
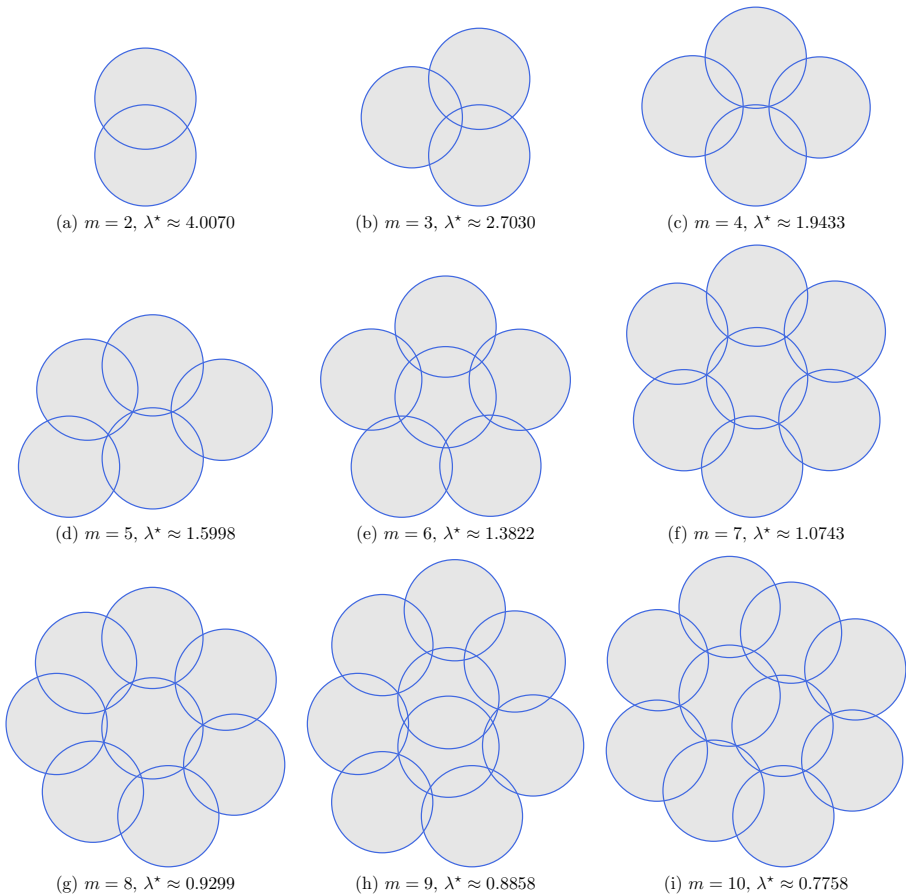
(a) $m = 2$, $\lambda^\star \approx 4.0070$ (b) $m = 3$, $\lambda^\star \approx 2.7030$ (c) $m = 4$, $\lambda^\star \approx 1.9433$

(d) $m = 5$, $\lambda^\star \approx 1.5998$ (e) $m = 6$, $\lambda^\star \approx 1.3822$ (f) $m = 7$, $\lambda^\star \approx 1.0743$

(g) $m = 8$, $\lambda^\star \approx 0.9299$ (h) $m = 9$, $\lambda^\star \approx 0.8858$ (i) $m = 10$, $\lambda^\star \approx 0.7758$

Fig. 2 Solution obtained by the application of Algorithm 2 starting from the best solution obtained by Algorithm 1 with $n_{\text{trials}} = 5000$ for $m \in \{2, 3, 4, 5, 6, 7, 8\}$ and $n_{\text{trials}} = 50{,}000$ for $m \in \{9, 10\}$

times of Algorithm 1 multiplied by the corresponding value of n_{trials} and adding the CPU time of Algorithm 2, is approximately a year of CPU time, almost entirely spent evaluating the objective function and its gradient. Naturally, in practice, the experiment was performed in a few days using a computer with multiple processors.

It is clear from Table 1 that for $m = 4$, $m = 5$, and $m = 10$ the solutions found by the application of Algorithms 1 and 2 are considerably better than the ones obtained by regular polygonal patterns, while the solutions are similar for the other values of m, with the exception of $m = 9$. For $m = 4$, $m = 5$, and $m = 10$, guided by the solutions found by the algorithm, we are able to foresee other regular patterns that could provide better solutions, as we describe next.

Table 1 Details of the application of Algorithm 1 followed by the application of Algorithm 2 starting from the best solution found by Algorithm 1 only. In instances with $m \leq 8$, $n_{\text{trials}} = 5000$ initial guesses were considered for Algorithm 1, while, in instances with $m = 9, 10$, $n_{\text{trials}} = 50{,}000$. Values in bold correspond to solutions that improve the solutions based on regular polygons

m	$\widehat{\lambda}$	Algorithm 1							Algorithm 2				
		$\lambda_1^\star$	$\|\nabla\lambda_1^\star\|_2$	#trial	it	fcnt	CPU time	Average CPU time	$\lambda_2^\star$	$\|\nabla\lambda_2^\star\|_2$	cycles	fcnt	CPU time
2	4.0070	4.0070	2.1E−01	632	7	43	13.54	17.09	4.0070	2.3E−01	1	1	0.32
3	2.7030	2.7030	2.0E−01	3621	22	47	28.88	63.93	2.7030	2.1E−01	1	2	1.21
4	1.9835	1.9433	2.5E−01	702	24	38	58.33	146.66	**1.9433**	2.6E−01	1	3	6.33
5	1.7380	1.6009	3.0E−01	2461	30	54	128.08	175.80	**1.5998**	2.9E−01	15	50	32.97
6	1.3803	1.3824	1.0E−01	2517	58	73	96.65	206.35	1.3822	1.1E−01	6	16	23.92
7	1.0645	1.1031	1.6E−01	719	67	77	181.41	232.49	1.0743	1.4E−00	71	255	1535.33
8	0.9118	0.9785	1.7E−01	811	85	105	274.15	261.23	0.9299	1.0E−00	97	352	2332.39
9	0.8313	0.9042	1.3E−01	48,378	94	108	278.21	313.15	0.8858	1.2E−01	96	292	1130.68
10	0.7829	0.8205	1.2E−01	8356	112	123	366.08	355.88	**0.7758**	1.0E−01	284	766	7268.30

4.3 Symmetric Solutions Inspired by Nonlinear Programming Solutions

The solutions for $m \in \{2, 3, 6, 7, 8\}$ shown in Fig. 2 suggest that the solutions following regular polygonal patterns illustrated in Fig. 1 for those values of m are optimal. The solutions for $m \in \{4, 5, 10\}$ displayed in Fig. 2 suggest that different types of solutions displaying regular patterns could be constructed by hand to improve on the solutions following regular polygonal patterns shown in Fig. 1. For $m = 9$ the algorithm could not recover a solution which is comparable with the regular polygonal pattern, and we were not able to improve this solution by hand. However, since the best solution was found at trial 48,378, this suggests that a better solution could be found by the algorithm by increasing n_{trials}. Also, the solutions found in Figs. 1h and 2h contain one and two balls in the inner layer, respectively. This indicates that the minimizer might actually feature two balls in the inner layer, but the algorithm is unable to get sufficiently close to this minimizer, due to the fact that the partial derivatives of λ with respect to the centers of the balls in the inner layer vanish.

For the case $m = 4$ we considered a configuration with the centers of the balls at the vertices of a diamond of side L and acute angle θ. Analogously to what was described in Sect. 4.1, we tested all values of $L \in [L_{\min}, L_{\max}]$ of the form $L = L_{\min} + kh(L_{\max} - L_{\min}), h = 1/(N-1)$, combined with all values of $\theta \in (0, \pi/2]$ of the form $\theta = \ell (\pi/2)/N$ for $k = 0, 1, \ldots, N-1$ and $\ell = 1, \ldots, N$, with $N = 10,000$. Figure 3a shows the result, and we observe a slight improvement compared to the result of Fig. 2c, which suggests optimality of this configuration.

For the case $m = 5$ we considered a configuration with the centers of four balls at the vertices of a diamond of side L and acute angle θ plus a fifth ball at the vertex of a coupled equilateral triangle. Figure 3b shows the result of varying L and θ as in the case $m = 4$. The figure and the associated value of λ improves with respect to the regular polygonal pattern of Fig. 1d, however the solution found with the nonlinear optimization process remains the best one.

As m increases, more balls will be placed in an internal layer and be surrounded by an external layer of balls in the optimal configuration. Hence, determining for which values of m an additional ball appears in the internal layer is an interesting question. Comparing the results of Fig. 1i and Fig. 2i suggests that a configuration with two balls instead of one in the internal layer could be better. Figure 2i also suggests that a better solution could be constructed for the case $m = 10$ by considering a subset of the hexagonal lattice

$$\mathcal{L}_r := \{kv_r + \ell w_r \mid (k, \ell) \in \mathbb{Z}^2\} \tag{20}$$

with $v_r := \frac{r}{2}(3, \sqrt{3})$, $w_r := \frac{r}{2}(3, -\sqrt{3})$, and $r = 1$; see [9, Fig.1]. We considered a configuration with an initial row with 3 balls, a second row with 4 balls and a third row with the remaining 3 balls. Figure 3c shows the configuration. The comparison with the value reported for a regular polygonal pattern in Fig. 1 shows that the eigenvalue corresponding to the hexagonal lattice is slightly smaller, but still larger than the solution found by the algorithm in Fig. 2i. As a curious fact, the value of λ for a configuration with $m = 5$ balls based on a hexagonal lattice is $\lambda \approx 1.7037$; see Fig. 3d. That value improves on the value associated with the regular pentagon (Fig. 1d) but
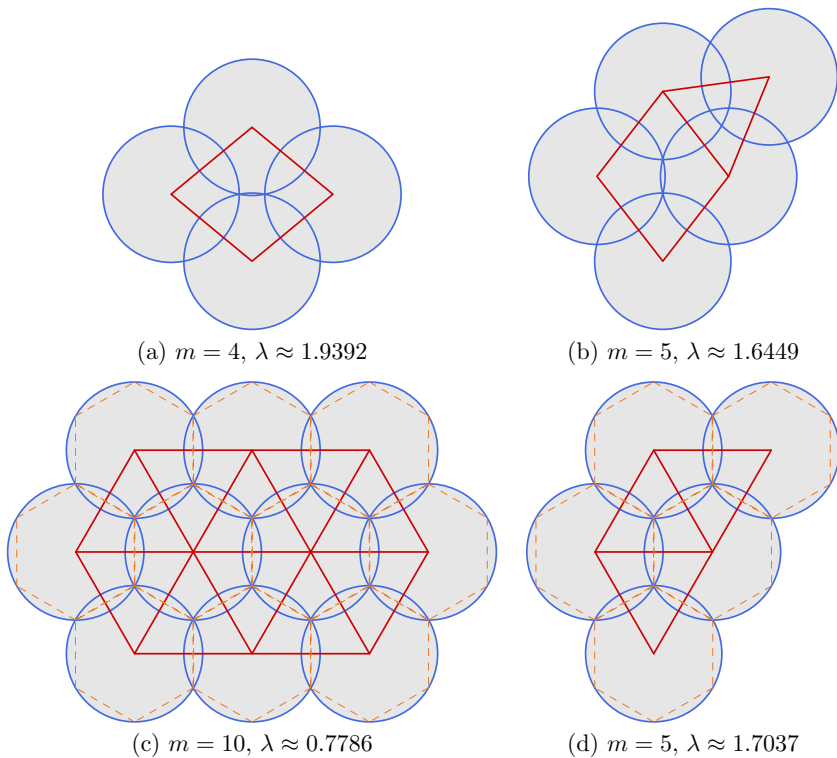
(a) $m = 4$, $\lambda \approx 1.9392$ (b) $m = 5$, $\lambda \approx 1.6449$

(c) $m = 10$, $\lambda \approx 0.7786$ (d) $m = 5$, $\lambda \approx 1.7037$

Fig. 3 Ad hoc symmetric solutions for $m \in \{4, 5, 10\}$. **a** The case $m = 4$ corresponds to a diamond with $L \approx 1.5408$ and $\theta \approx 1.3509$. The case $m = 5$ depicted in **b** corresponds to a "combination" of the solutions for $m = 3$ and $m = 4$, i.e., a diamond with $L \approx 1.5408$ ad $\theta \approx 1.3509$ and the fifth ball's center in the vertex of an equilateral triangle. **c** The case $m = 10$ corresponds to a subset of the regular hexagonal lattice with $L = 1$. The case $m = 5$ depicted in **d** also corresponds to a subset of the same lattice

is worse than that associated with the diamond plus equilateral triangle (Fig. 3b) and also worse than that found by the optimization process (Fig. 2d), which continues to be the best.

To summarize our results, our analysis suggests the following best candidates for a solution of the problem for $m \in \{2, \ldots, 10\}$:

m = 2: The solution found with the balls centered at the extremes of a segment of length $L \approx 1.1212$ depicted in Fig. 1a.

m = 3: The solution associated with the equilateral triangle of side $L \approx 1.5015$ depicted in Fig. 1b.

m = 4: The solution associated with a diamond shape of side $L \approx 1.5408$ and acute angle $\theta \approx 1.3509$ depicted in Fig. 3a.

m = 5: The non-regular solution found by applying Algorithms 1 and 2, depicted in Fig. 2d, with centers

$$(0, 0), (0, 1.83912168353), (-1.29145209709, 1.35732348664),$$

$(-1.65126893885, -0.162712427424)$, $(1.36903341977, 0.960875323247)$.

m = 6, 7, 8, 9: The regular $(m-1)$-gon with a single ball in the inner layer and with side $L \approx 1.7878, 1.7238, 1.5625, 1.4138$, respectively; see Fig. 1e–h.

m = 10: The non-regular solution found by applying Algorithms 1 and 2, depicted in Fig. 2i, with centers:

$(0, 0)$, $(0, 1.80125448879)$,

$(1.07646612984, -2.3856843472)$, $(-1.43149832049, -1.09446805145)$,

$(-0.308292621733, -1.87884265359)$, $(2.43012959985, -1.27436971318)$,

$(1.04596189888, -0.596401635114)$, $(2.4823402281, 0.522706233573)$,

$(-1.41569186399, 0.696839479126)$, $(1.21471563231, 1.24472165911)$.

5 Conclusions and Future Works

In this work we have investigated the problem of minimizing the first Dirichlet Laplacian eigenvalue with respect to a union of balls with fixed identical radii and varying centers. We have shown that this problem presents interesting challenges and open questions. In addition to contributing to the field of eigenvalue optimization by investigating a new type of geometrical constraint, the techniques developed in this work constitute a basis for the study of other shape optimization problems involving PDEs where the set is defined as a union of moving components, a topic of growing interest as shown by the recent developments of the method of Moving Morphable Component/Void [25, 42]. Unlike shape optimization problems with moving components where no PDEs are involved, such as covering problems, the singularities appearing in the solution of the PDE due to the nonsmoothness and nonconvexness of $\Omega(\boldsymbol{x})$ play a fundamental role for the mathematical analysis of the problem and for the numerical approximation of solutions, as the gradient of the solution may become unbounded close to singular configurations. From the numerical point of view, we observed that the singularities preclude the apparition of small holes in $\Omega(\boldsymbol{x})$ during the optimization process, which limits the possible evolutions of $\Omega(\boldsymbol{x})$ and makes reaching a minimizer difficult. The singularities in this problem are particularly strong due to the Dirichlet conditions, and milder singularities can be expected for other type of PDEs such as problems involving a piecewise constant conductivity.

Further investigations should therefore be focused on proposing alternatives to the numerical algorithms in order to deal with these strong singularities. This could be achieved in several ways, by relaxation of the PDE as in [14] for instance, or by regularization of the shape. Improving the precision for the calculation of the eigenvalue and of its gradient as well as providing error estimates with guaranteed accuracy should be a primary task in order to obtain better approximations of the minimizers. From the theoretical point of view, proving the existence of second-order derivatives of $\boldsymbol{x} \mapsto \lambda(\boldsymbol{x})$ is an interesting problem, for which the techniques developed in [37] could be used. The Hessian of $\boldsymbol{x} \mapsto \lambda(\boldsymbol{x})$ could then be employed to certify that some candidates are local minimizers. This approach has been successfully applied

recently for the minimization of the first Dirichlet eigenvalue in the class of n-gons in [12]. For problem (3), the existence of a boundary expression for the second-order shape derivative of $\Omega \mapsto \lambda(\Omega)$ is not always guaranteed, as shown in [37] for a similar problem, due to the fact that $\Omega(x)$ is nonsmooth and nonconvex.

For $m \leq 10$, we have produced a list of plausible candidates for minimizers that can be used as a reference for future investigations, either to mathematically prove that they are indeed local or global minimizers, or to propose better candidates via numerical experiments. Determining minimizers for $m \geq 11$ seems challenging, as numerical experiments show that the inner layer of the minimizer contains two or more balls, which tend to stay motionless due to the occurrence of singularities when small gaps appear in $\Omega(x)$. In this case, sets that are close to, or equal to a subset of the regular hexagonal lattice seem to provide good candidates, as shown by the case $m = 10$.

References

1. Agarwal, P.K., Pach, J., Sharir, M.: State of the union (of geometric objects). In: Surveys on Discrete and Computational Geometry. Contemporary Mathematics, vol. 453, pp. 9–48. American Mathematical Society, Providence (2008)
2. Akçelik, V., Biros, G., Ghattas, O., Keyes, D., Ko, K., Lee, L.-Q., Ng, E.G.: Adjoint methods for electromagnetic shape optimization of the low-loss cavity for the international linear collider. J. Phys. Conf. Ser. **16**(1), 435 (2005)
3. Allaire, G., Aubry, S., Jouve, F.: Eigenfrequency optimization in optimal design. Comput. Methods Appl. Mech. Eng. **190**(28), 3565–3579 (2001)
4. Amaral, V.A., Andreani, R., Birgin, E.G., Marcondes, D.S., Martínez, J.M.: On complexity and convergence of high-order coordinate descent algorithms for smooth nonconvex box-constrained minimization. J. Glob. Optim. **84**, 527–561 (2022)
5. Amstutz, S., Novotny, A.A.: Topological optimization of structures subject to Von Mises stress constraints. Struct. Multidiscip. Optim. **41**(3), 407–420 (2009)
6. Antunes, P.R.S.: Is it possible to tune a drum? J. Comput. Phys. **338**, 91–106 (2017)
7. Antunes, P.R.S., Freitas, P.: Numerical optimization of low eigenvalues of the Dirichlet and Neumann Laplacians. J. Optim. Theory Appl. **154**(1), 235–257 (2012)
8. Birgin, E.G., Laurain, A., Massambone, R., Santana, A.G.: A shape optimization approach to the problem of covering a two-dimensional region with minimum-radius identical balls. SIAM J. Sci. Comput. **43**, A2047–A2078 (2021)
9. Birgin, E.G., Gardenghi, J.L., Laurain, A.: Asymptotic bounds on the optimal radius when covering a set with minimum radius identical balls. Technical Report, MCDO180422. Institute of Mathematics and Statistics, University of São Paulo, São Paulo (2022)
10. Birgin, E.G., Laurain, A., Massambone, R., Santana, A.G.: A shape-Newton approach to the problem of covering with identical balls. SIAM J. Sci. Comput. **44**(2), A798–A824 (2022)
11. Birgin, E.G., Martínez, J.M.: Practical Augmented Lagrangian Methods for Constrained Optimization. Society for Industrial and Applied Mathematics, Philadelphia (2014)
12. Bogosel, B., Bucur, D.: On the polygonal Faber–Krahn inequality. arXiv e-prints (March 2022). arXiv:2203.16409
13. Bogosel, B., Henrot, A., Lucardesi, I.: Minimization of the eigenvalues of the Dirichlet–Laplacian with a diameter constraint. SIAM J. Math. Anal. **50**(5), 5337–5361 (2018)
14. Bogosel, B., Velichkov, B.: A multiphase shape optimization problem for eigenvalues: qualitative study and numerical results. SIAM J. Numer. Anal. **54**(1), 210–241 (2016)
15. Bourdin, B., Bucur, D., Oudet, É.: Optimal partitions for eigenvalues. SIAM J. Sci. Comput. **31**(6), 4100–4114 (2009/2010)
16. Bucur, D.: Minimization of the k-th eigenvalue of the Dirichlet Laplacian. Arch. Ration. Mech. Anal. **206**(3), 1073–1083 (2012)

17. Bucur, D., Giacomini, A.: Minimization of the k-th eigenvalue of the Robin–Laplacian. J. Funct. Anal. **277**(3), 643–687 (2019)
18. Conway, J.H., Sloan, N.J.A.: Sphere packings, lattices and groups. In: Grundlehren der mathematischen Wissenschaften [Fundamental Principles of Mathematical Sciences], vol. 290, 3rd edn. Springer, New York (1999)
19. Costabel, M., Dauge, M.: Singularities of electromagnetic fields in polyhedral domains. Archive for Rational Mechanics and Analysis **151**(3), 221–276 (2000)
20. Daniel-Noreland, J.O., Rajitha-Udawalpola, M., Martin-Berggren, O.: A hybrid scheme for bore design optimization of a brass instrument. J. Acoust. Soc. Am. **128**(3), 1391 (2010)
21. De Philippis, G., Lamboley, J., Pierre, M., Velichkov, B.: Regularity of minimizers of shape optimization problems involving perimeter. J. Math. Pures Appli. Neuvième Sér. **109**, 147–181 (2018)
22. Delfour M.C., Zolésio, J.-P.: Shapes and Geometries. Advances in Design and Control, vol. 22, 2nd edn. Society for Industrial and Applied Mathematics (SIAM), Philadelphia (2011)
23. Edelsbrunner, H.: The union of balls and its dual shape. Discrete Comput. Geom. **13**(3–4), 415–440 (1995)
24. Fremiot, G., Sokolowski, J.: The structure theorem for the Eulerian derivative of shape functionals defined in domains with cracks. Siberian Math. J. **41**, 974–993 (2000)
25. Guo, X., Zhang, W., Zhang, J., Yuan, J.: Explicit structural topology optimization based on moving morphable components (MMC) with curved skeletons. Comput. Methods Appl. Mech. Eng. **310**, 711–748 (2016)
26. Hecht, F.: New development in FreeFem++. J. Numer. Math. **20**(3–4), 251–265 (2012)
27. Henrot, A.: Extremum Problems for Eigenvalues of Elliptic Operators. Frontiers in Mathematics. Birkhäuser Verlag, Basel (2006)
28. Henrot, A., Oudet, E.: Minimizing the second eigenvalue of the Laplace operator with Dirichlet boundary conditions. Arch. Ration. Mech. Anal. **169**(1), 73–87 (2003)
29. Henrot, A., Pierre, M.: Shape Variation and Optimization. EMS Tracts in Mathematics, vol. 28. European Mathematical Society (EMS), Zürich (2018)
30. Hintermüller, M., Kao, C.-Y., Laurain, A.: Principal eigenvalue minimization for an elliptic problem with indefinite weight and Robin boundary conditions. Appl. Math. Optim. **65**(1), 111–146 (2012)
31. Kedem, K., Livne, R., Pach, J., Sharir, M.: On the union of Jordan regions and collision-free translational motion amidst polygonal obstacles. Discret. Comput. Geom. **1**(1), 59–71 (1986)
32. Kevin, S.: On shape optimization with non-linear partial differential equations. PhD thesis, Technische Universität Berlin (2014)
33. Khludnev, A.M., Sokolowski, J.: The Griffith formula and the Rice–Cherepanov integral for crack problems with unilateral conditions in nonsmooth domains. Eur. J. Appl. Math. **10**, 379–394 (1999)
34. Kozlov, V.A., Maz'ya, V.G., Rossmann, J.: Elliptic Boundary Value Problems in Domains with Point Singularities. Mathematical Surveys and Monographs, vol. 52. American Mathematical Society, Providence (1997)
35. Lamboley, J., Laurain, A., Nadin, G., Privat, Y.: Properties of optimizers of the principal eigenvalue with indefinite weight and Robin conditions. Calc. Var. Partial Differ. Equ. **55**(6), Art. 144, 37 (2016)
36. Lamboley, J., Novruzi, A., Pierre, M.: Estimates of first and second order shape derivatives in nonsmooth multidimensional domains and applications. J. Funct. Anal. **270**, 2616–2652 (2016)
37. Laurain, A.: Distributed and boundary expressions of first and second order shape derivatives in nonsmooth domains. J. Math. Pures Appl. Neuvième Sér. **134**, 328–368 (2020)
38. Maz'ya, V., Nazarov, S., Plamenevskij, B.: Asymptotic Theory of Elliptic Boundary Value Problems in Singularly Perturbed Domains. Vol. I. Operator Theory: Advances and Applications, vol. 111 . Birkhäuser Verlag, Basel (2000)
39. Sokołowski, J., Zolésio, J.-P.: Introduction to Shape Optimization. Springer-Verlag, Berlin (1992)
40. Šverák, V.: On optimal shape design. J. Math. Pures Appl. Neuvième Sér. **72**(6), 537–551 (1993)
41. Wright, S.J.: Coordinate descent methods. Math. Program. **151**, 3–34 (2015)
42. Zhang, W., Li, D., Zhou, J., Du, Z., Li, B., Guo, X.: A Moving Morphable Void (MMV)-based explicit approach for topology optimization considering stress constraints. Comput. Methods Appl. Mech. Eng. **334**, 381–413 (2018)
43. Zhu, S., Hu, X., Liao, Q.: Convergence analysis of Galerkin finite element approximations to shape gradients in eigenvalue optimization. BIT **60**(3), 853–878 (2020)